Renew. Energy Environ. Sustain. **9**, 5 (2024)

https://doi.org/10.1051/rees/2024003

Renewable Energy and Environmental Sustainability

Available online at:
www.rees-journal.org

Research Article

Open Access

Evaluation of the electrical parameters and performance of floating PV generators

Cristiana B. Maia[1*], Antonia Sônia A.C. Diniz[1], Saulo Amador Bonfim[1], and Lawrence L. Kazmerski[2]

[1] Graduate Program in Mechanical Engineering, Pontifical Catholic University of Minas Gerais, Belo Horizonte, Brazil
[2] Renewable and Sustainable Energy Institute (RASEI), University of Colorado Boulder, Boulder, Colorado, 80309 – USA

Received: 28 August 2023 / Received in final form: 26 December 2023 / Accepted: 28 January 2024

Abstract. This study provides evaluation of floating photovoltaics (PV) in the Brazil tropical climate and discusses the specific technical and environmental benefits and limitations. This paper develops a model simulating the annual performance of the photovoltaic generator of a floating photovoltaic plant as a function of a given conditions. The reference is a 1.2-MWp floating-PV system commissioned in 2023 near the city of Grão Mogol, Brazil, in the reservoir of the PCH Santa Marta hydropower plant. The influence of the ambient meteorological and marine parameters on the PV module temperature, current, voltage, and power were evaluated. The simulation uses a reference crystalline-Si PV module and the Engineering Equation Solver (EES). Relevant experimental data, including incident solar radiation, ambient temperature, and wind speed were used as input data for the model. The effect of these parameters on the thermal end electrical parameters was assessed. Although small variations were found throughout the year, significant hourly and daily variations were observed, depending on solar irradiation and ambient and resulting module surface temperatures. The voltage at the maximum power decreases with the increase of the solar module surface temperature. The convective heat transfer rates are higher than the radiative heat transfer rates. This study provides a first-time complete energy and exergy analysis of a floating PV system (FPVS) incorporating the various heat transfer rates, electrical and irradiance parameters, under climate and meteorological conditions for this Brazil location.

Keywords: Photovoltaics / floating PV / floatovoltaics / modeling / characterization

1 Introduction and background

In 2022, the renewable share of electricity supply grew by 9%, representing a 29.9% share of the global electricity generation [1,2]. Among the renewable resources, solar energy stands out as a compelling solution for growing energy demands with a clean and abundant supply [1–5]. Among the renewable sources, photovoltaics (PV) has dominated the electric power sector over the past few years. More than 240 GW of solar PV power (~70% of the renewable power total) was installed during 2022—with a cumulative 1-TW reached early in the year [1,2]. Though the technology growth and advancements have been significant, PV power additions will need to nearly triple to meet the IEA net-zero emissions targets by 2030 [4,5]. This calls for accelerating and expanding implementation of solar PV in a wide range of new and/or underutilized sectors [1,5,6]. One such option is to expand electricity production on available water areas (reservoirs, lakes) through the use of floating-PV (also termed "floatovoltaic") systems (FPVS) [7,8].

Most PV systems require intensive land utilization of about 10-m^2 for each kW produced [1]. In densely populated countries, PV systems are many times installed in areas that are potential priorities for other purposes. The rationale for the use of these aquatic areas is based on the unavailability of suitable land-based regions or avoiding diminishing critical land areas for agricultural production, housing, or commercial operations. A floating PV system also offers significant technical benefits such as decreasing the operating temperature of the solar generators leading to higher electrical-power outputs [9]. The floating systems can help control the unwanted growth of algae, stimulate the aquatic life, and lowering the loss of needed water due to evaporation. Estimations are that a floating 1-MW of power plant avoids the evaporation of approximately 20,000 m^3 of water per year [2]. In moorlands, marshes, or bogs, floating-PV can lead to restoration these waste areas for specialized agricultural development. Offshore, this

* e-mail: cristiana@pucminas.br

option is beginning to be used to enhance aquaculture. The installation of such "floatovoltaics" on existing hydroelectric operations provides cost benefits through the complementary use of existing transmission and distribution systems [10]. Additionally, the generated PV electricity can be used to pump water back into the reservoir (pumped storage) that can provide value to the hydroelectric installation during periods of water shortage or drought. There are some disadvantages of FPVS, such as the higher difficulties found on the design and construction of the systems, the decrease on the water quality due to the presence of the modules, and the increase on the risks of damage due to stress and vibration on the modules in floating conditions [11].

Currently, the market for FPVS is relatively small, but is expanding rapidly. Most projects are located in Asia, but it is estimated that more than 60 countries have projects under development or operation, with a total global capacity of approaching 3-GWp in 2022 [3]. Numerous studies have been already conducted, but it is important to develop more research on the topic.

Some studies focused on ways to enhance the efficiency of FPVS and/or to reduce it costs. Sutanto et al. [12] introduced a passive cooling system and estimated the increase of electrical power due to this thermosiphon. Compared to ground PV generation, the power output increased about 7.9%, and compared to conventional FPVS, the increase was about 3.3%. A comparison between ground and floating PV systems, for monofacial and bifacial modules, was developed by Yakubu et al. [13]. The bifacial gain of ground PV systems and FPVS was, respectively, 2.51% and 4.57%. Nevertheless, the authors observed that the additional energy generated by the bifacial system is not significant enough to justify the installation of a new system. Choi et al. [14] developed an experimental analysis of the influence of the wind speed on floating modules, concluding that the higher effect is observed in the boundaries. The authors suggested that lower cost materials can be used in the middle regions of the array, which can lead to a 19% manufacturing cost for a 2.5 MW system. Zhang et al. [15] presented a methodology for the design and verification of FPVS operating in coastal marine conditions. The system was tested with a 5 MW pilot project installed in Singapore.

Numerical simulations are extensively used by researchers for predicting the behavior of systems with complex mathematical models, obtaining results for a wide range of boundary conditions. A numerical simulation of the heat transfer coefficients was developed by Tina et al. [4], who used these data to simulate and compare monofacial and bifacial FPVS. Computational Fluid Dynamics (CFD) was used to obtain values for the global coefficients of heat transfer over FPVS, quantifying the cooling effect caused by the water body. The authors concluded that the water temperature does not affect significantly the cell temperature [5]. Kichou et al. developed an approach for the evaluation of the performance of FPVS, combining Matlab and Rhino/Grasshoper environments [16]. The authors assessed the influence of module temperature, albedo, modules spacing and inclination, and the effect of a tracking mechanism.

The objective of this study is to provide a first-time complete energy and exergy analysis of an FPVS. An exergy analysis of thin-film solar PV modules was reported by Kumar [6] for ground-mount, floating, and submersed modules. The analysis was performed using experimental data obtained in small devices, for one day. Higher exergy losses were found for ground-mount PV when compared to floating and submersed PV systems. The authors did not develop an energy analysis. The module temperature was predicted by Rahaman et al. [7] using three different approaches: thermal, empirical, and computational fluid dynamics (CFD) models. The models were simulated for specific periods and compared with experimental data for a single module installed in Passauna Lake in Brazil. Although an energy balance for the estimation of the surface temperature of the module is included, the model does not cover both an energy and exergy efficiency.

This paper comprises a theoretical analysis of the performance of an FPVS (Veredas Sol e Lares) near the city of Grão Mogol, Brazil (Fig. 1). A mathematical model was developed for the prediction of the module surface temperature, the heat transfer rates, and the energy and exergy efficiencies of the module, using actual experimental data of solar radiation, ambient temperature, and wind speed as input data for the FPVS location. The electrical performance of the module was also assessed. The hourly analysis and evaluation have been performed for a one-year period. The main objective of the paper is to estimate the thermal and electrical parameters of a FPVS, to predict its performance for the city of Grão Mogol, Brazil. The mathematical model can be adapted for other locations, using their meteorological data.

2 Methodology

2.1 Mathematical model

The incident radiation on a tilted PV module G_T is given by equation (1) [8]:

$$G_T = G_b R_b + G_d\left(\frac{1+\cos\beta}{2}\right) + G\rho_g\left(\frac{1-\cos\beta}{2}\right), \quad (1)$$

G_b, G_d, and G stand for the beam, diffuse, and global components of the incident solar radiation on a horizontal plane (in W/m^2). β is the slope angle of the module, assumed as 27° to maximize the energy during the winter [8], ρ_g is the ground reflectance, assumed as 6.5%, and R_b is a geometric factor defined as the ratio of beam radiation on the tilted surface to that on a horizontal surface, given by equation (2) [8]:

$$R_b = \frac{\cos\theta}{\cos\theta_z}, \quad (2)$$

θ is the angle of incidence of solar radiation (in°), and θ_z is the zenith angle (in°). The angle of incidence, for the southern hemisphere, is given by equation (3) [8]:

$$\cos\theta = \cos(\phi+\beta)\cos\delta\cos\omega + sen(\phi+\beta)sen\delta \quad (3)$$

Fig. 1. Floating 1.2 MW PV system (Veredas Sol e Lares) located on reservoir near Grão Mogol, Brazil.

ϕ, δ, and ω stand for the latitude of the location, the declination, and the hour angle, all in°. The zenith angle is given by equation (4) [8]:

$$\cos\theta_z = \cos\phi\cos\delta\cos\omega + sen\,\phi\,sen\,\delta \tag{4}$$

The declination (in°) can be found by equation (5) [8]:

$$\delta = 23.45\,sin\left[\frac{360}{365}(284+n)\right] \tag{5}$$

where n stands for the nth day of the year.

The incident solar radiation heats the module surface, and heat is lost by convection and radiation by the top and bottom surfaces, as indicated in Figure 2. There is a convective heat loss for the ambient air and a radiative heat loss for the sky by the top surface. From the bottom surface, there is a convective heat loss for the air and a radiative heat loss for the water surface. The heat transfer model was based on [10,17,18].

The convective and radiative heat transfer rates from the top surface of the module are given (in W) by equation (6) and (7), respectively:

$$Q_{convs} = h_s A(T_m - T_a), \tag{6}$$

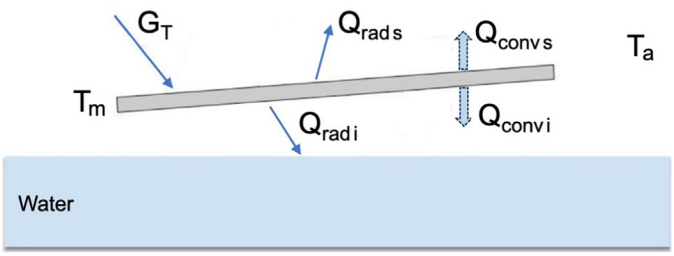

Fig. 2. Schematic representation of the heat transfer.

$$Q_{rads} = h_{rs}A(T_m - T_{sky}) \tag{7}$$

h_s and h_{rs} are the convective and radiative coefficients, both in W/(m^{2}K). T_m is the temperature (in K) of the module surface of area A (in m^2), T_a and T_{sky} are the temperatures of the ambient air and the sky (in K), respectively.

The temperature of the module surface is defined by equation (8) [17]:

$$T_m = T_a + \left[\frac{G_T}{U_o + U_1 V}\right], \tag{8}$$

V is the wind speed (in m/s), and U_0 e U_1 are heat loss coefficients both in W/(m^{2}K). Average values of 24.9 W/m^{2}K and 7.55 W/m^{2}K are recommended [17].

The top surface convective heat transfer represents a combination of natural and forced convection [19]. The convective coefficient is determined based on the Nusselt number Nu_s, equation (9)

$$Nu_s = \frac{h_s L}{k}, \tag{9}$$

where Nu_s is determined based on the Nusselt numbers of natural and forced convection, obtained from literature correlations, by equation ((10)) [20]:

$$Nu_s^3 = Nu_{Ns}^3 + Nu_{Fs}^3, \tag{10}$$

in which L is the module length (in m) and k, the thermal conductivity of the air (in W/(m,K)).For Reynolds numbers between 10^1 and 10^6, there are no sudden variations in the laminar and turbulent boundary layers over a flat plate. Therefore, the Nusselt number of the forced convection is given by equation (11) [10]:

$$Nu_{Fs}^2 = Nu_L^2 + Nu_T^2, \tag{11}$$

Nu_L, and Nu_T, represent the Nusselt numbers for laminar and turbulent flow, respectively. The laminar Nusselt is given by equation (12) [10]

$$Nu_L = 0.664\, Re^{0.5} Pr^{1/3}, \tag{12}$$

Pr is the Prandtl number Re is the Reynolds number based on the module length (equation (13)) [10]:

$$Re = \frac{VL}{\nu}, \tag{13}$$

V is the wind speed (in m/s) and v is the kinematic viscosity of the air (in m^2/s).

The turbulent Nussel is (equation (14)) [10]

$$Nu_T = \frac{\xi/8\, Re.Pr}{1 + 12.7(\xi/8)^{0.5}(Pr^{2/3} - 1)}, \tag{14}$$

ξ is the friction factor, given by equation (15) [10]

$$\xi/8 = 0.037 Re^{-0,2}, \tag{15}$$

For the natural convection, the correlation of Churchill and Chu (equation 15), presented by [20], is valid for laminar and turbulent flows, for Rayleigh between 10^{-1} and 10^{12} [10].

$$Nu_{Ns} = \left\{0.825 + 0,387[Ra \cos\beta\, \phi(Pr)]^{1/6}\right\}^2, \tag{16}$$

β is the slope angle (in°) of the module and Ra is the Rayleigh number, given by equation (17) [20].

$$Ra = \frac{g(T_m - T_a)L^3}{\nu\alpha T_f}, \tag{17}$$

T_f is the film temperature (in K), evaluated as the average between the module surface and the ambient temperatures. α is the thermal diffusivity of the air (in m^2/s).and g is the gravitational acceleration, 9.81 m/s^2.

The function $\phi(Pr)$ is evaluated by equation (18) [10]:

$$\phi(Pr) = \left[1 + (0.492/Pr)^{9/16}\right]^{8/27}, \tag{18}$$

The radiative coefficient (in $W/(m^2K)$) is given by equation (19) [20]

$$h_{rs} = \varepsilon\sigma\left(T_m^2 + T_{sky}^2\right)\left(T_m + T_{sky}\right), \tag{19}$$

ε is the surface emittance, assumed as 0.88. σ is the Stefan-Boltzmann constant,

$$\sigma = 5.67 \times 10^{-8}\, \mathrm{W/m^2K^4},$$

T_{sky} is the sky temperature (in K), given by equation (20) [21]:

$$T_{sky} = 0.0552\, T_a^{1,5}, \tag{20}$$

In on-ground PV systems, the energy balance in the bottom surface only considers convective heat transfer rates for the ambient air. In floating PV systems, it is required to take into account also the radiative heat transfer rates between the bottom surface and the water. The convective and radiative heat transfer rates from the bottom surface of the module are, respectively (equation 21) and (22):

$$Q_{convi} = h_i A(T_m - T_a), \tag{21}$$

$$Q_{radi} = h_{ri} A\left(T_m - T_{sky}\right), \tag{22}$$

The convective coefficient is determined based on the Nusselt number Nu_i (equation 23)

$$Nu_i = \frac{h_i L}{k}, \tag{23}$$

where the Nusselt is given by equation (24) [20]:

$$Nu_i^3 = Nu_{Ni}^3 + Nu_{Fi}^3, \tag{24}$$

Nu_{Ni}, and Nu_{Fi}, represent the Nusselt numbers for natural and forced convection, respectively. For the bottom surface, the expressions are given by equation

(25) and (26) [18].

$$Nu_{Fi} = 0.86Re^{1/2}Pr^{1/3}, \tag{25}$$

$$Nu_{Ni} = \begin{matrix} 0.76Ra^{1/4} & if\, 1 \times 10^4 < Ra < 1 \times 10^7 \\ 0.15Ra^{1/3} & if\, 1 \times 10^7 < Ra < 3 \times 10^7 \end{matrix}, \tag{26}$$

The Rayleigh number is given by equation (27) [20]:

$$Ra = \frac{g(T_f - T_a)L^3}{\nu\alpha T_f}, \tag{27}$$

T_f is the film temperature (in K), given by equation (28) [18]

$$T_f = T_a + 0,25\,(T_m - T_a), \tag{28}$$

The radiative coefficient is (equation 29) [18]

$$h_{ri} = \frac{\sigma.F_{PV}\left(T_m^2 + T_w^2\right)(T_m + T_w)}{1/\varepsilon_{PV} + 1/\varepsilon_w - 1}, \tag{29}$$

T_w is the water surface temperature (in K), ε_w, e ε_{PV}, are the water and module emittances, assumed as 0.91 and 0.96, respectively. F_{PV}, is the view factor, assumed as 1.

The performance of the module can be assessed using energy and exergy analysis. The energy efficiency is defined as the ratio of the energy generated by the PV module to the incident solar radiation [16], and is determined by equation (30) [16].

$$\eta = \frac{V_{oc}.I_{sc}}{G_T A}, \tag{30}$$

The open circuit voltage V_{oc}, (in V) and the short-circuit current I_{sc}, (in A) are defined by equation (31) and (32) [22]

$$I_{sc} = I_{sc,ref}\left(\frac{G_T}{G_{ref}}\right) + \alpha\left(T_m - T_{m,ref}\right), \tag{31}$$

$$V_{oc} = V_{oc,ref} - \beta_v\left(T_{m,ref} - T_m\right) + A\,ln\left(\frac{G_T}{G_{ref}}\right), \tag{32}$$

$I_{sc,ref}$, and $V_{oc,ref}$, represent the open circuit voltage (in V), and short circuit current (in A), under standard test conditions, given in the PV module datasheet. α is the temperature coefficient for the short circuit current, β_v is the temperature coefficient for the open circuit voltage and A is the modified ideality factor (equation 33) [22]

$$A = \frac{nkT_m}{q}, \tag{33}$$

n is the diode ideality factor, k is the Boltzmann constant ($1.38 \times 10^{-23}\,J/K$,) and q is the electric charge of one electron ($1,602 \times 10^{-19}\,C$,). G_{ref}, and $T_{m,ref}$, represent the reference solar radiation and module surface temperature, respectively, 1000 W/m^2 and 25 °C.

The exergy efficiency (equation 34) is the ratio of the lost exergy (determined as the difference between the electric and thermal exergies) to the solar exergy [16]:

$$\psi = \frac{V_m I_m - (1 - T_a/T_m)h_s A(T_m - T_a)}{(1 - T_a/T_{sun})G_T A} \bullet FF, \tag{34}$$

T_{sun} is the sun temperature, assumed as 5800 K, and FF is the fill factor, defined as (equation 35) [16]

$$FF = \frac{P}{V_{oc}I_{sc}}, \tag{35}$$

Nevertheless, this is a standard definition, based only on convective heat losses through the top surface of the PV module. Considering both convective and radiative thermal losses, through the top and bottom surfaces, the thermal exergy rate $\dot{E}_{xt}$, (in W), can be rewritten as Eq, (36)

$$\begin{aligned} \dot{E}_{xt} = {} & (1 - T_a/T_m)h_s A(T_m - T_a) \\ & + \left(1 - T_a/T_{sky}\right)h_{rs}A\left(T_m - T_{sky}\right) \\ & + (1 - T_a/T_m)h_i A(T_m - T_a) \\ & - (1 - T_a/T_w)h_{ri}A(T_m - T_w), \end{aligned} \tag{36}$$

Therefore, the exergy efficiency is given by equation (37):

$$\frac{\psi = V_m I_m - \dot{E}_{xt}}{(1 - T_a/T_{sun})G_T A \bullet FF,} \tag{37}$$

The power generated by the PV module P (in W), (equation 38) is given as the product of the maximum power point voltage V_m, (in V), and current I_m, (in A), (equation 39 and 40).

$$P = V_m I_m, \tag{38}$$

$$I_m = I_{m,ref}\left(\frac{G_T}{G_{ref}}\right), \tag{39}$$

$$V_m = V_{m,ref} - \beta_{vm}\left(T_{m,ref} - T_m\right), \tag{40}$$

$I_{m,ref}$, and $V_{m,ref}$, are the maximum power point voltage and current under standard test conditions, given in the PV module datasheet.

The reference PV module has a width of 0.483 m and a length of 1.172 m.

2.2 Materials and methods

The PV module was simulated for the city of Grão Mogol (latitude 16° 33' 27" S and longitude 42° 53' 38" W), where the floating PV plant is located on the lake of the CEMIG-hydroelectric power plant Santa Marta. The floating PV plant has an area of 11,000 m^2, with 3,050 PV modules, and an installed power of 1.2 MWp, able to supply energy to approximately 1250 families in 21 cities. Grão Mogol has an Aw (Equatorial savannah with dry winter) climate,

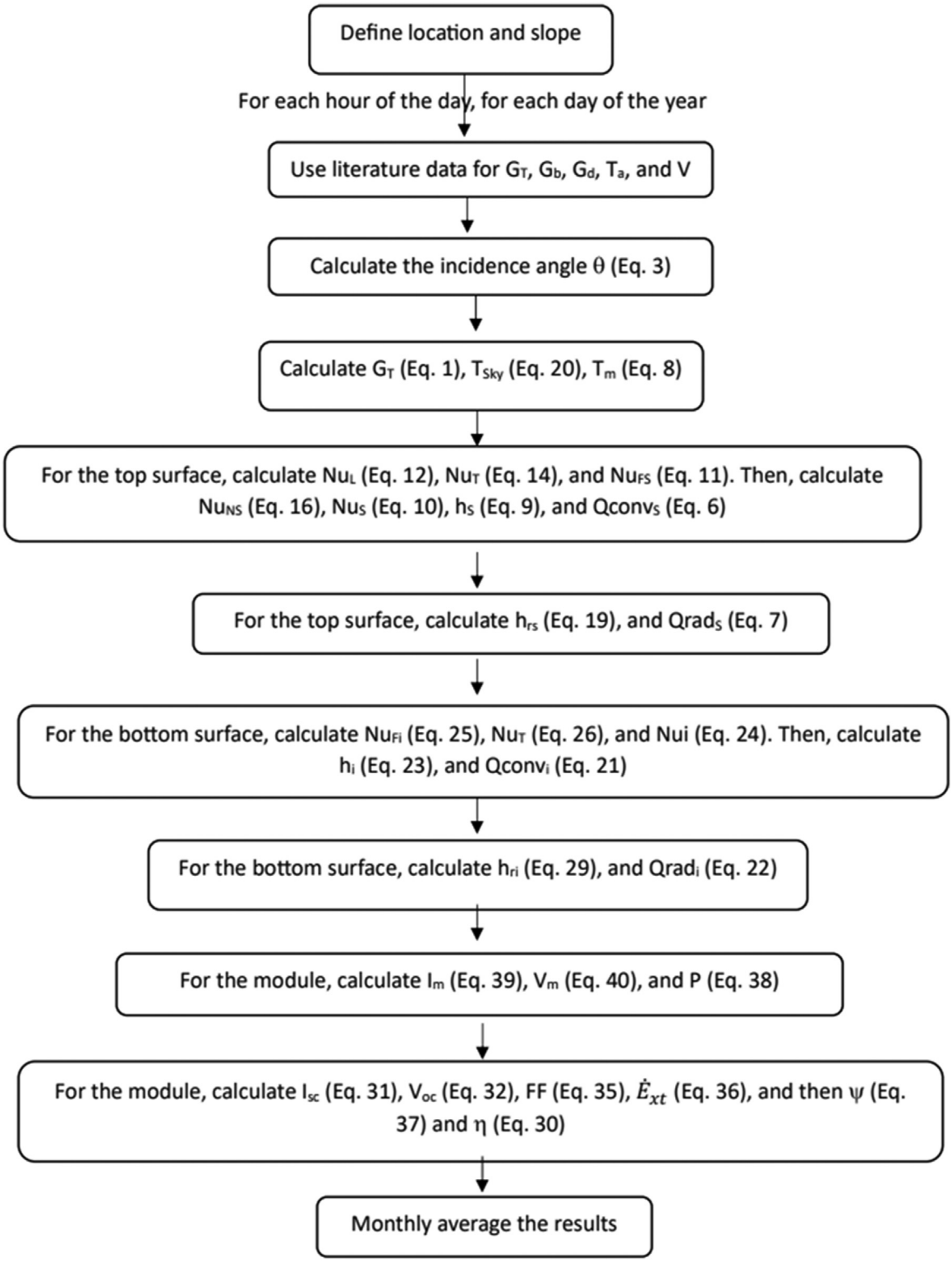

Fig. 3. Schematics flowchart.

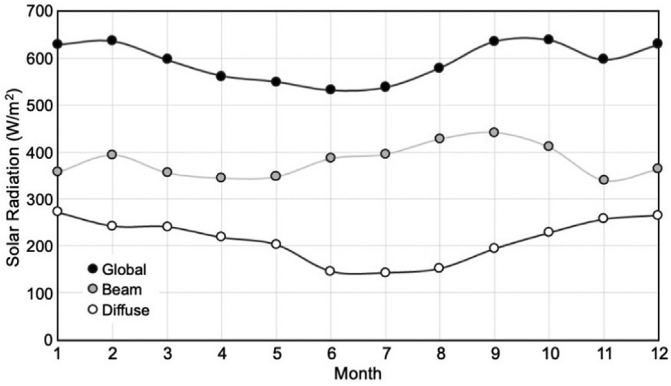

Fig. 4. Monthly averaged solar radiation.

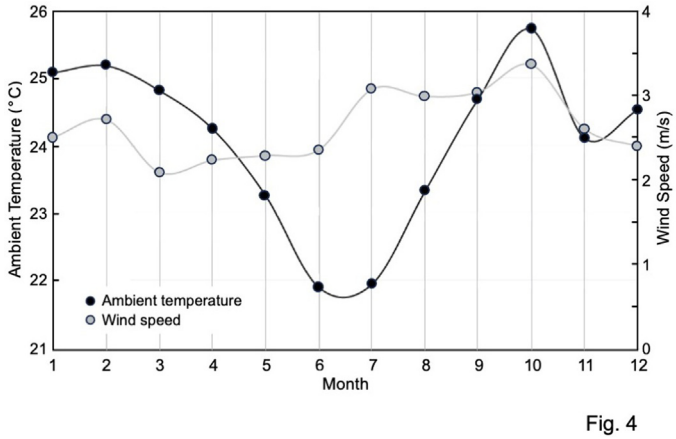

Fig. 5. Monthly averaged ambient temperature and wind speed.

according to the Koppen-Geiger climate classification [23,24]. The Equatorial savannah climate presents a monthly average temperature above 18 $°C$ for all the months. The dry winter classification implies a dry winter season, with precipitation below 60 mm, representing less than 4% of the yearly total precipitation.

Experimental data of solar radiation, ambient temperature, and wind speed were obtained from the literature [25] for the city of Grão Mogol, Brazil, and used as input data to run the mathematical model developed. Figure 3 presents a flowchart of the steps followed in the equations set. The data were obtained on an hourly basis, and the monthly averaged results are presented in Figures 4 and 5.

The highest values for total solar radiation are found between September and March, corresponding to spring and summer in the Southern Hemisphere. The diffuse component is lower for the winter, which is consistent with the Aw climate, with dry winter and lower incidence of clouds. The ambient temperature follows the behavior of solar radiation, with higher values during spring and summer. When considering the average values of wind speed, there are no significant variations, with a range between 2.1 and 3.4 m/s. However, when the absolute values are assessed, the range expands to 0.1 to 10.3 m/s.

3 Results

Based on the experimental data from ambient conditions, it was possible to estimate the behavior of the FPVS operating in Grão Mogol. The results are presented for one day of simulation, on an hourly basis, and on a monthly average basis.

3.1 Daily results

To evaluate the unsteady behavior of the FVPS, the system was simulated for one specific day, selected as the spring equinox, September 21st for the southern hemisphere. According to [26] the solar radiation collected on this day has little difference from the annual average. Figure 6 shows the global, beam, and diffuse components of solar radiation for the spring equinox, obtained on an hourly basis. The relatively low levels of diffuse radiation show

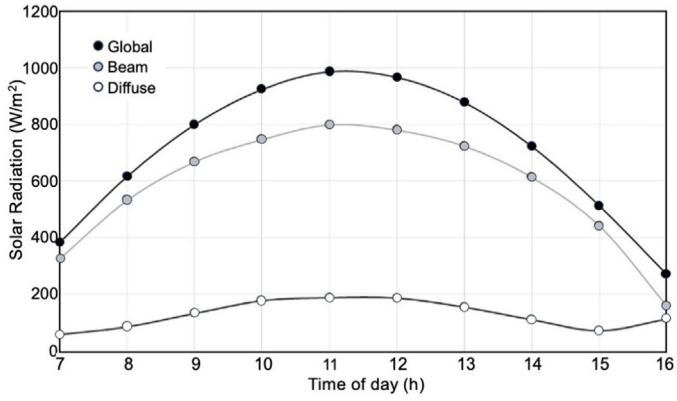

Fig. 6. Spring equinox in Grão Mogol, Brazil: Hourly radiation during time period.

that it was a clear day, with a high clearness index. The highest global solar radiation was approximately 990 W/m^2. It is important to mention that the values presented in this section represent the daily variation of the variables. The results presented in Figures 4 and 5 stand for the monthly averaged values, which presented a smaller variation.

The ambient temperature and wind speed are shown in Figure 7, as well as the module surface temperature. The minimum and maximum ambient temperatures were, respectively, 20.0 and 27.8 $°C$, consistent with the high solar radiation levels. The wind speed varied throughout the day, ranging between 1.0 and 3.9 m/s. The module surface temperature presented lower values at the beginning and end of the day when the solar radiation was lower.

The power generated by the PV module depends on the incident solar radiation and the ambient temperature during the spring equinox. Since it was a clear day, both parameters presented similar behaviors, increasing during the morning and decreasing during the afternoon. Therefore, the power generated showed similar behavior, as shown in Figure 8. The energy efficiency depends on the

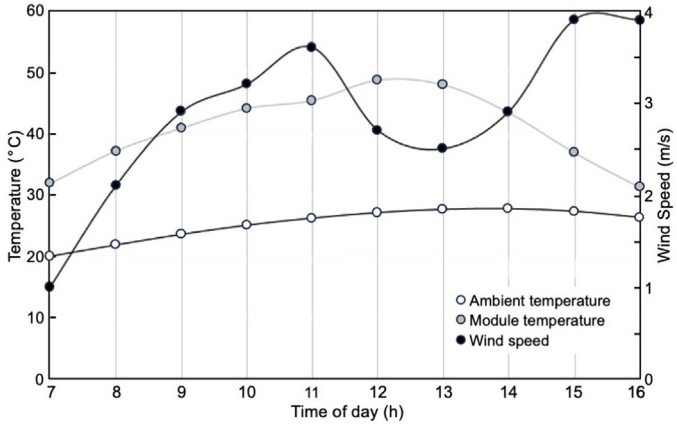

Fig. 7. Spring equinox in Grão Mogol, Brazil: Ambient and module temperatures and wind speed during time period.

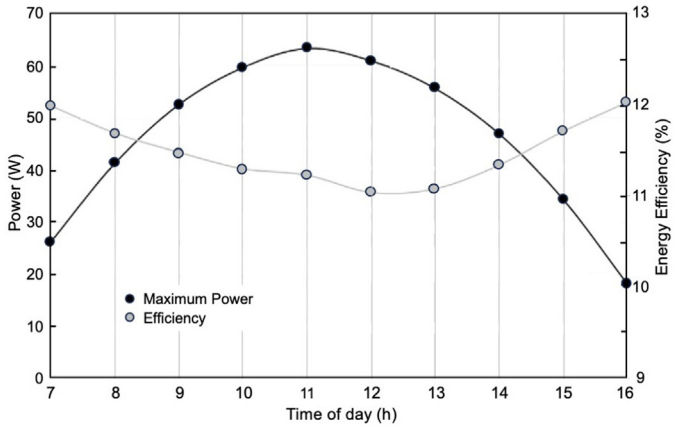

Fig. 8. Hourly PV power and energy efficiency.

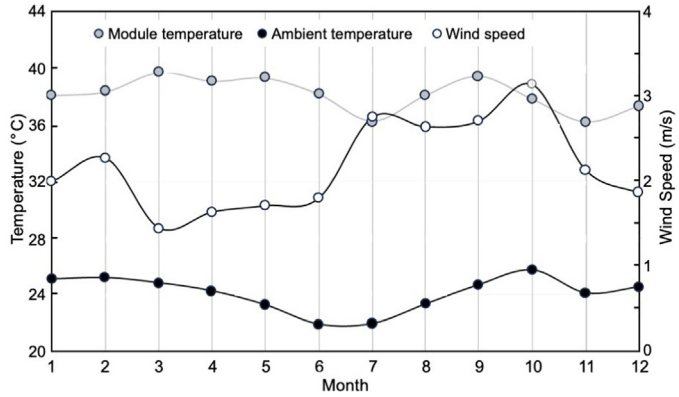

Fig. 9. Monthly averaged ambient temperature and wind speed.

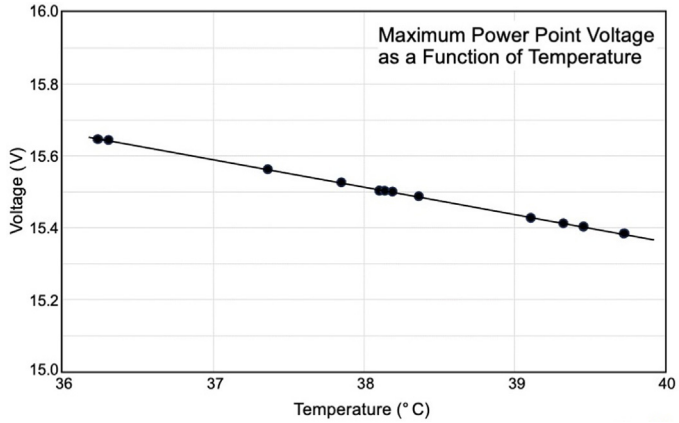

Fig. 10. Module voltage at the maximum power point.

open circuit voltage V_{oc}, and the short-circuit current I_{sc},. The open circuit voltage did not present significant variations, and the short circuit current increased during the morning and decreased in the afternoon. However, the variations of the solar radiation were more significant than the short circuit current, and the energy efficiency presented a trend opposite to the power generated.

3.2 Annual results

The results were obtained on an hourly basis. To evaluate the long-term behavior of the FPVS, monthly averaged results are presented. The module surface temperature depends on the incident solar radiation, ambient temperature, and wind speed. The monthly average temperature did not present significant variations throughout the year, since the higher ambient temperature and solar radiation levels occurred with higher wind speeds, and the effects were balanced, as observed in Figure 9. The voltage at the maximum power point is shown in Figure 10. It decreases with the increase in solar module surface temperature, as expected.

Figure 11 presents the power delivered by the FPVS. As already discussed, the parameter that most influences the power is the incident solar radiation; therefore, the power delivered follow the same general behavior of the incident solar radiation. Although the daily variations are high, the monthly averaged values do not vary significantly.

The monthly averaged heat fluxes are shown in Figure 12. The convective heat fluxes at the inferior and superior surfaces (conv I and conv s), the radiative heat fluxes at the inferior and superior surfaces (rad i and rad s), and the global heat transfer fluxes at the inferior and superior surfaces (q i and q s) are defined in Figure 2. When comparing the heat transfer modes, it can be seen that the convective heat transfer is higher than radiative heat transfer, on both surfaces. When comparing the inferior and superior surfaces, the heat transfer fluxes are higher on the superior surfaces. As expected, the heat transfer increases with the increase of the solar radiation in the morning and decreases when the solar radiation decreases in the afternoon.

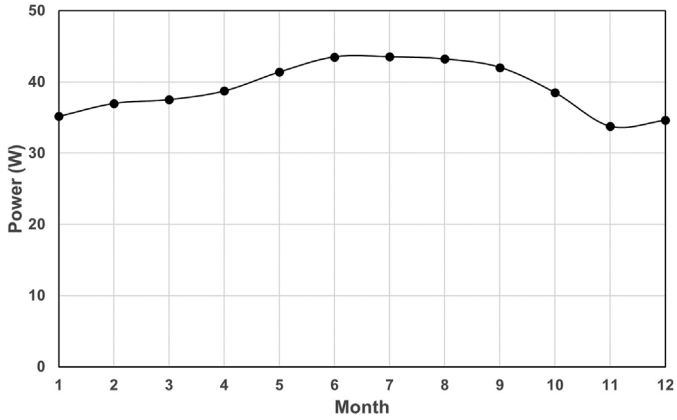

Fig. 11. Power delivered.

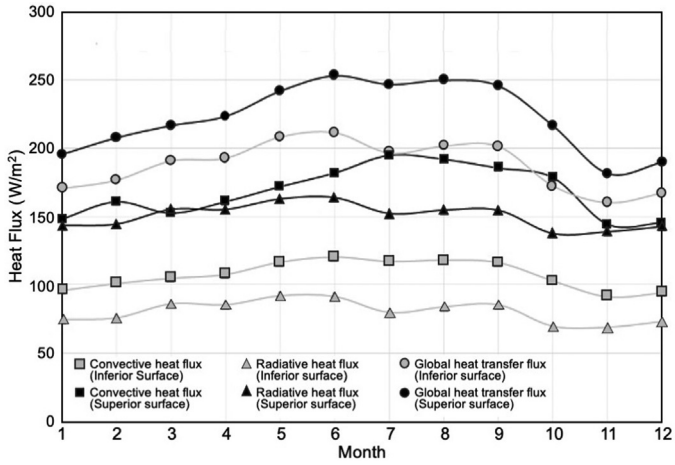

Fig. 12. Monthly averaged heat fluxes.

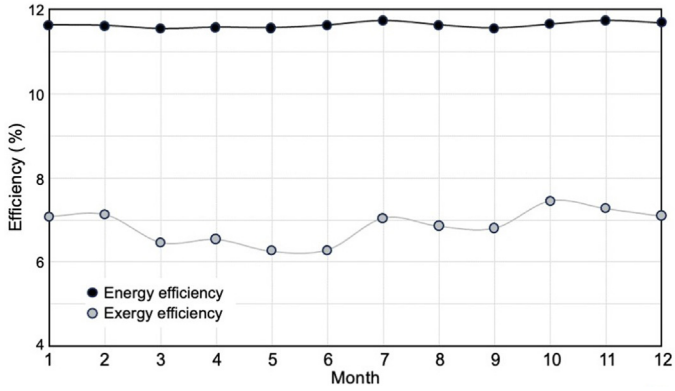

Fig. 13. PV module efficiencies.

The energy and exergy efficiencies are shown in Figure 13. Energy efficiency is the ratio of the energy generated by the PV module to the incident solar radiation. The energy generated by the PV module is the product between the open circuit voltage, which did not present significant variations, and the short circuit current, which varied similarly to the incident solar radiation. Therefore, as the energy generated and the incident solar radiation presented similar behavior, the energy efficiency was nearly constant, with an average value of 11.5%. It is worth mentioning, however, that although the monthly averaged energy efficiency did not present significant variations, it varies during the day (Fig. 8), presenting an opposite trend of the power generated.

The exergy efficiency showed an inverse trend to the incident solar radiation. As expected, the energy efficiency is higher than the exergy efficiency. Energy is the ability of a substance to perform work, and exergy gives the maximum work that a substance can perform. Therefore, energy and exergy efficiencies are different. The energy efficiency of a PV system depends on the generated electricity and the total energy input based on the total solar irradiation. The exergy efficiency stresses that both external losses and internal irreversibilities need to be addressed to improve performance. Higher exergy efficiency reflects higher energy quality used in the system, which makes the system more sustainable [19].

4 Conclusions

This paper presented an analysis of the performance of a floating crystalline-Si PV module, in conjunction with a FPVS installed in Grão Mogol, Brazil. Experimental data of solar radiation, ambient temperature, and wind speed were used as input data for the model. Thermal and electrical parameters were evaluated, and an energy and exergy analysis of the system was performed.

The primary results include:

- Although the variations throughout the year were small, significant variations of the parameters during the day were found.
- For maximum monthly average incident solar radiation of 640 W/m^2,, wind speed of 3.4 m/s and ambient temperature of 25.7 ,, the maximum monthly average module surface temperature was 39.7 ,.
- For the spring equinox, for a maximum incident solar radiation of 987 W/m^2,, wind speed of 3.9 m/s and ambient temperature of 27.8 ,, the maximum module surface temperature was 48.7 ,. with maximum power of 63.3 W.
- As expected, the voltage at the maximum power point decreases with the increase in solar module surface temperature.
- The convective heat transfer rates are higher than the radiative heat transfer, on both surfaces, but higher on the superior surfaces. The yearly average convective heat flux was 138 W/m^2, and the yearly average radiative heat flux was 115 W/m^2,.
- The energy efficiency is higher than the exergy efficiency and presents a trend opposite to the power generated. The maximum monthly average energy and exergy efficiencies were 11.7%, in July, and 7.5%, in October, respectively.

The purpose of this research study was to develop a mathematical model to predict the annual performance of a FPVS operating in Grão Mogol. Overall, the results indicate that the system has the potential to play a crucial role in the efficient use of the water body to generate energy, at the same time that reduces the water evaporation of the lake. Although the mathematical model has been developed for a specific location in Brazil, the developed methodology can be applied to the design and evaluation of FPVS elsewhere with appropriate experimental data available from the literature of the site-specific conditions.

Acknowledgements

This study was supported in part by the Coordenação de Aperfeiçoamento de Pessoal de Nível Superior - Brasil (CAPES) - Finance Code 001. We appreciate the help of GREEN PUC Minas for technical and facilities assistance. The authors are also thankful to CEMIG, PUC Minas, FAPEMIG, Fulbright Scholar Program, and CNPq for their technical assistance, encouragement, and support for this research project.

Funding

The funding support of the Fulbright Scholar Program, FAPEMIG, CNpq and CAPES-MEC was provided for portions of this research.

Conflict of Interest

The authors declare that they have no conflict of interest.

Author contribution statement

Conceptualization, C.M., A.D.. and L.K.; Methodology, C.M.; Investigation, S.B.; Writing – Original Draft Preparation, C.M.; Writing – Review & Editing, A.D. and L.K.; Visualization, S.B; Supervision, C.M.; Project Administration, A.D.; Funding Acquisition, A.D. and L.K.

Data availability statement

The data that support the findings of this study are available on request from the corresponding author.

References

1. A. El Hammoumi, A. Chalh, A. Allouhi, S. Motahhir, A. El Ghzizal, A. Derouich, Design and construction of a test bench to investigate the potential of floating PV systems, J. Clean. Prod. **278**, (2021)
2. M. Rosa-Clot, G.M. Tina, S. Nizetic, Floating photovoltaic plants and wastewater basins: An Australian project, Energy Procedia, (2017)
3. REN, Renewables in Cities 2021 Global Status Report, 2021. [Online]. Available: https://www.ren21.net/wp-content/uploads/2019/05/GSR 2021_Full_Report.pdf
4. G.M. Tina, F. Bontempo Scavo, L. Merlo, F. Bizzarri, Comparative analysis of monofacial and bifacial photovoltaic modules for floating power plants, Appl. Energy, **281**, (2021)
5. D. Lindholm, J. Selj, T. Kjeldstad, H. Fjær, V. Nysted, CFD modelling to derive U-values for floating PV technologies with large water footprint, Sol. Energy, **238**, 238–247 (2022)
6. N.M. Kumar, U. Subramaniam, M. Mathew, A. Ajitha, D.J. Almakhles, Exergy analysis of thin-film solar PV module in ground-mount, floating and submerged installation methods, Case Stud. Therm. Eng. **21**, (2020)
7. A. Rahaman et al., Floating photovoltaic module temperature estimation: modeling and comparison, Renew. Energy, **208**, 162–180 (2023)
8. J.A. Duffie, W.A. Beckman, *Solar engineering of thermal processes: fourth edition*. (2013)
9. K.S. Hayibo, J.M. Pearce, Foam-based floatovoltaics: a potential solution to disappearing terminal natural lakes, Renew. Energy, **188**, (2022)
10. K. Yaman, G. Arslan, A detailed mathematical model and experimental validation for coupled thermal and electrical performance of a photovoltaic (PV) module, Appl. Therm. Eng. **195**, (2021)
11. E. Tercan, M.A. Dereli, B.O. Saracoglu, Location alternatives generation and elimination of floatovoltaics with virtual power plant designs, Renew. Energy, **193**, (2022)
12. B. Sutanto, Y.S. Indartono, A.T. Wijayanta, H. Iacovides, Enhancing the performance of floating photovoltaic system by using thermosiphon cooling method: numerical and experimental analyses, Int. J. Therm. Sci. **180**, (2022)
13. R.O. Yakubu, D.A. Quansah, L.D. Mensah, W. Ahiataku-Togobo, P. Acheampong, M.S. Adaramola, Comparison of ground-based and floating solar photovoltaic systems performance based on monofacial and bifacial modules in Ghana, Energy Nexus, **12**, (2023)
14. S.M. Choi, C.D. Park, S.H. Cho, B.J. Lim, Effects of wind loads on the solar panel array of a floating photovoltaic system – experimental study and economic analysis, Energy **256**, (2022)
15. C. Zhang, J. Dai, K.K. Ang, H.V. Lim, Development of compliant modular floating photovoltaic farm for coastal conditions, Renew. Sustain. Energy Rev. **190**, 114084 (2024)
16. A.K. Pandey, V.V. Tyagi, S.K. Tyagi, Exergetic analysis and parametric study of multi-crystalline solar photovoltaic system at a typical climatic zone, Clean Technol. Environ. Policy, **15**, (2013)
17. L. Micheli, The temperature of floating photovoltaics: case studies, models and recent findings, Sol. Energy, **242**, 234–245 (2022)
18. P. Yang, L.H.C. Chua, K.N. Irvine, J. Imberger, Radiation and energy budget dynamics associated with a floating photovoltaic system, Water Res. **206**, (2021)
19. I. Dincer, A. Abu-Rayash, Chapter 6 - Sustainability modeling, in: I. Dincer, A. Abu-Rayash (Eds.), *Energy Sustainability, Academic Press*, 2020, pp. 119–164
20. A. Bejan, *Convection heat transfer: fourth edition*. (2013)
21. W.C. Swinbank, Long-wave radiation from clear skies, Q.J. R. Meteorol. Soc. **89**, 339–348 (1963)
22. A. Chouder, S. Silvestre, N. Sadaoui, L. Rahmani, Modeling and simulation of a grid connected PV system based on the evaluation of main PV module parameters, Simul. Model. Pract. Theory, **20**, (2012)
23. M.C. Peel, B.L. Finlayson, T.A. McMahon, Updated world map of the Köppen-Geiger climate classification, Hydrol. Earth Syst. Sci. **11**, 1633–1644 (2007)
24. M.S. Reboita, M. Rodrigues, L.F. Silva, M.A. Alves, Aspectos climáticos do estado de Minas Gerais, Rev. Bras. Climatol. **18**, 307–326 (2016)
25. Pvsyst, PVsyst: Software for the Study and Simulation of Photovoltaic Systems, 2023. www.pvsyst.com
26. F.J. Collado, Quick evaluation of the annual heliostat field efficiency, Sol. Energy, **82**, (2008)

Cite this article as: Cristiana B.Maia, Antonia Sônia A.C. Diniz, Saulo Amador Bonfim, and Lawrence L. Kazmerski.2024. Evaluation of the electrical parameters and performance of floating PV generators, Renew. Energy Environ. Sustain. **9**, 5 (2024)